EFDA–JET–PR(09)34

M. Baruzzo, B. Alper, T. Bolzonella, M. Brix, P. Buratti, C.D. Challis, F. Crisanti, E de la Luna, P.C. de Vries, C. Giroud, N.C. Hawkes, D.F. Howell, F. Imbeaux, E. Joffrin, H.R. Koslowski, X. Litaudon, J. Mailloux, A.C.C Sips, O. Tudisco and JET EFDA contributors

NTM Magnetic Spectrum and Magnetic Coupling in JET Tokamak

NTM Magnetic Spectrum and Magnetic Coupling in JET Tokamak

M. Baruzzo[1], B. Alper[3], T. Bolzonella[1], M. Brix[3], P. Buratti[2], C.D. Challis[3], F. Crisanti[2], E de la Luna[6,8], P.C. de Vries[3], C. Giroud[3], N.C. Hawkes[3], D.F. Howell[3], F. Imbeaux[5], E. Joffrin[5,8], H.R. Koslowski[4], X. Litaudon[5], J. Mailloux[3], A.C.C Sips[7,8], O. Tudisco[2] and JET EFDA contributors*

JET-EFDA, Culham Science Centre, OX14 3DB, Abingdon, UK

[1]Consorzio RFX, EURATOM-ENEA Association, Corso Stati Uniti 4, 35127 Padova, Italy
[2]Associazione Euratom/ENEA sulla Fusione, CP 65-00044 Frascati, Rome, Italy
[3]EURATOM-CCFE Fusion Association, Culham Science Centre, OX14 3DB, Abingdon, OXON, UK
[4]Forschungszentrum Jülich GmbH, Association EURATOM-FZ Jülich, Institut für Plasmaphysik, Trilateral Euregio Cluster, D-52425 Jülich, Germany
[5]CEA, IRFM, F-13108 Saint-Paul-lez-Durance, France.
[6]Laboratorio Nacional de Fusión, Asociación EURATOM-CIEMAT, Madrid, Spain
[7]European Commission, Brussels, B-1094, Belgium
[8]EFDA-CSU, Culham Science Centre, OX14 3DB, Abingdon, OXON, UK
** See annex of F. Romanelli et al, "Overview of JET Results", (Proc. 22 [nd] IAEA Fusion Energy Conference, Geneva, Switzerland (2008)).*

Preprint of Paper to be submitted for publication in
Plasma Physics and Controlled Fusion

ABSTRACT.
An experimental study on the poloidal mode number (m) spectrum produced by a single toroidal mode number (n) Neoclassical Tearing Mode in JET tokamak is presented, Clear evidence of the existence of more than one significant m components is given. The analysis is performed comparing several methods and diagnostics; among the latter we mention high frequency magnetic pick up coils and Electron Cyclotron Emission radiometer, which measures detailed electron temperature radial profiles at high time resolution. The two diagnostics are also used together in a cross coherence calculation technique. The issue of the interaction of this multiple m structure with the plasma is addressed as well, with particular attention paid to plasma toroidal rotation and rotation shear, obtained from Charge Exchange Spectroscopy data. This effect has been studied under different operational plasma scenarios on JET in order to investigate both dependencies on plasma parameters, and consequences on the scenario itself.

1. INTRODUCTION

The efficiency and performance of fusion devices can be limited by various classes of magneto hydro dynamic instabilities. The main parameter which is linked to devices efficiency is $\beta = 2\mu_0 p/B$, which is the ratio between plasma kinetic pressure and total magnetic field pressure. From this parameter another one could be derived, which has the expression $\beta_N = 100\beta aB/I$, with a minor radius, B total magnetic field and I total plasma current in MA. This parameter is often used in tokamaks physics, since it takes into account also the work that the magnetic perturbation has to do against magnetic tension to displace magnetic field lines.

Neoclassical Tearing Modes (NTMs) [1] are among the most dangerous magneto hydro dynamic instabilities in fusion plasmas, because they limit the maximum reachable β_N value and hence the discharge performance. Studying the physics of onset and growth of these modes is of great importance both for physical understanding and for scenario development, in particular when high β_N operation advanced scenarios are concerned.

Large efforts have been made to study the stability and the various triggering mechanisms for these modes [2], and the dependency of the impact they have on confinement as a function of their radial position [3].

In this paper, instead, the different problem of the determination of the whole NTM spatial structure will be faced, in particular we will focus on the composition of the poloidal (m) number spectrum. Toroidal curvature and poloidal shaping effects introduce sidebands of the main m component that can interact among each other and with the plasma, especially in high β_N plasmas with a highly elliptic and triangular shape.

Clearly these sidebands, having different m numbers from the main one, might resonate inside the plasma at different radial positions: for example an $m = 2$ mode with $n = 1$ toroidal mode number has toroidicity-induced $m = \pm 1$ sidebands, whose phase fronts match field line winding where the winding index $q = (m + 1)/n = 1$ *and* $q = (m-1)/n = 1$.

Sidebands might then cause forced magnetic reconnection on different resonant surfaces, giving rise to secondary magnetic islands, that in turn could degrade the plasma confinement properties. A particular care will be given in treating this point, to verify whether this is the case for the JET tokamak.

The picture created so far could give a new point of view to understand the stability properties of these modes, since the presence of a resonant tearing mode can act to damp plasma rotation, which itself is one of the actors that are involved in the mode stability.

In section 2 an experimental coherence-based technique to measure NTM radial structure will be described, in section 3 the application of the technique to two different advanced scenario pulses will be shown, and the results will be cross checked with toroidal rotation data as well. In section 4 the overall picture will be discussed, showing how to extract sidebands information from the measured radial structure with some ad-hoc simple modelling; in section 5 conclusions will be drawn.

2. EXPERIMENTAL SETUP AND TECHNIQUE DESCRIPTION

Important information about NTMs physics is given by the radial profile of the magnetic field perturbation produced by the mode inside the plasma, and also by the radial localization of the island associated to the mode, that can act directly on plasma flow and local transport. In order to obtain these quantities, a time-frequency domain coherence technique [4] was implemented between two different diagnostic measurements: a set of wideband magnetic pick up coils and a set of 48 electron temperature signals from the Electron Cyclotron Emission (ECE) fast radiometer.

In this section the experimental technique will be described using some viewgraphs as examples, these plots will be then used in the following sections as well, and commented in their physical meaning there.

The magnetic pick up coils used have a bandwidth of 1 MHz and are composed by titanium wire wounded in 70 turns onto an alumina ceramic former, with a return wire trough the center of the coil. They have an effective area of $0.064 m^2$, are placed inside the torus vacuum vessel and are protected by a stainless steel case, the plasma facing component is itself protected by a carbon tile case. The array used for n-number analysis is located at a major radius value R=3.88m, at a vertical position of $Z = 1.05m$ and at different toroidal angles between $\phi = 77.00^o - 110.38^o$.

The ECE radiometer can perform a local measurement of the radial profile of electron temperature and its temporal behaviour, with a radial separation between channels of 2−4cm along a line of sight, which is about 13cm under the plasma mid plane, and with a measurement window that covers the machine region R>2.6m, with respect to an overall machine radial extension from 1.82m to 3.87m. The detector can be set for either X-mode or O-mode radiation acquisition, giving a reliable measurement for a toroidal field $B_\varphi \geq 1.7T$ [5]. The acquisition system has up to 500kHz bandwidth, and each channel can store 6 mega-samples, this feature makes the diagnostic suitable to high frequency wavelet and coherence analysis, and convenient to follow mode evolution in a large diagnostic time window [6].

The technique, that makes use of both these diagnostics, is based on the observation that the equilibrium perturbation by a rotating magnetic island induces a particular pattern in temperature profile oscillations, in such a way that oscillations of magnetic signals are linked to the temperature oscillations inside the plasma [7], and coherence phase radial profile shows a π-jump whenever an island is crossed moving along the plasma radius. The last effect is due to the radial displacement of magnetic field lines produced by the rotating island, that has opposite directions on the outer side of the island x-point than on the inner side of the x-point. This standard analysis method has been recently elaborated and implemented on JET to be executed in a totally unattended way, and it is now one of the standard tools for NTM study.

The approach starts from *n*-number analysis of magnetic signals (Figure 1), which assigns an *n*-number to each bin in the time-frequency domain and provides a basis to filter out the temperature oscillations which are not linked to the selected n-number perturbation. Then an automatic algorithm for mode tracking in the time-frequency domain is used to follow the frequency evolution for each *n* mode number, this procedure also gives the absolute amplitude of each mode in the magnetic signal.

The tracking algorithm searches for maxima of magnetic amplitude in well defined *n* time-frequency bins, and then follows the maximum forward and backward in its time-frequency evolution, this process is repeated for each *n* number from 1 to 4. A check on mode amplitude continuity is implemented as well, to discriminate between cyclic and continuous modes.

The calculation of coherence amplitude and phase in Fourier space between one magnetic signal and each ECE channel is performed using Welch's method, the mode frequency provided by the tracking algorithm is used to calculate coherence just in the frequency bin of the mode, in order to increase signal to noise ratio and to reduce the computing time. The following step is an algorithm designed to find the radial position of phase jumps for each time slice and for each mode. Particular care was taken to discard low coherence amplitude temporal frames and couple of points too far one from each other. An example of a coherence phase and amplitude radial profile is shown in Figure 2, the coherence phase changes smoothly from the high field side to the low field side, according to the fact that the poloidal (θ) angle changes along the line of sight, and a double jump in the low field side can be observed as well. Both of these features will be explained in the next sections.

The last step is an algorithm producing a signal with island radius as a function of time. For this aim a tracking algorithm is used, similar to the one used to detect mode frequency in the magnetic signals, which follows in time the maximum value in space-time density of phase jump points. More than one iteration of this process is used to find NTMs position, in this way multiple tracks for each mode can be found, until a maximum number of three [8]. Again particular care was taken to avoid picking up phase jumps due to noise, using a cross check with coherence cross spectrum at that radius, to find a fluctuation amplitude sensibly larger then noise value.

The main systematic uncertainty of this technique arises in the determination of the radial positions of ECE channels, which depends on the accuracy of magnetic field profile reconstruction including plasma current and diamagnetic contributions; at low magnetic field also the refraction can be

relevant and its effects on the island position has been evaluated by a ray-tracing code. A characterization of these systematic errors on channels position, which in turn reflects in the same error on modes localization, is ongoing using different temperature diagnostics and different NTM localization techniques as well [8]. The estimated radial resolution of individual channels is 2–5cm for typical JET plasma parameters [5].

After this the temperature fluctuation auto-spectrum can be calculated (Figure 3), and can be used in a rough approximation, together with temperature gradients, to estimate the periodic displacement of magnetic surfaces due to island rotation, which is in turn linked to island width and mode magnetic amplitude.

3. EXPERIMENTAL OBSERVATIONS

3.1 N=1 NTMS

In this section the outputs of the previously described technique will be exposed for two different pulses, following the logical order of the various analysis steps, and links will be drawn to rotation data analysis.

The first example of the use of the method is shown for JET Pulse No: 77590, which is characterized by a 2.1MA plasma current, a 2.7T toroidal field, $\beta_N = 2.2$, and an Advanced Tokamak scenario with a high triangularity configuration and a total heating power of approximately 30MW subdivided in 20MW of neutral beam power, 7MW of Ion Cyclotron Resonance Heating (ICRH) and 2.5MW of Lower Hybrid wave heating (LH) [9]. External input power and β_n traces are shown in Figure 4 upper and mid plot.

This is one of the Advanced Tokamak configurations developed at JET in the last years, where a considerable effort has been made for the tailoring of the magnetic q profile, to achieve a rather flat q in the center of the plasma, with the minimum value of q around 2.

Despite the aim of the tailoring effort was to obtain a higher MHD stability, MHD events still happens in this type of scenario, also given the natural evolution of the q profile towards its relaxed state, and they can have very detrimental effects on plasma global confinement. In Figure 4, where the integrated $n = 1$ (red) and $n = 2$ (blue) magnetic signals from tangential pick up coils are shown in the bottom plot, it is clear that the peak in $n = 1$ activity around 6.5s is then reflected on a drop in β_n from 2.3 to 1.8, which is in turn an evidence for a considerable drop in confinement, given the constant input power coupled to the plasma.

From the magnetic spectrogram (Figure 1) the presence of two NTMs during the heating phase is highlighted. In fact an early NTM appears at 4.2s and is identified by the green *n*=3 track, then a larger 2/1 NTM (in red) appears at 6.5s and remains in the plasma for the rest of the heating phase. In Figure 3 a contour plot is shown of the cross amplitude between each ECE channel and a single magnetic coil at the frequency of the mode magnetic fluctuation. The plot displays two high fluctuation amplitude traces at the high field side at 2.75m and at the low field side at 3.4m, that are due to the same magnetic surface crossing twice the ECE line of sight. Moving towards a larger

normalized radius a contrast with a dark zone can be observed, followed by another bright zone with high fluctuation amplitude. This typical structure gives us preliminary information on the island position, since the displacement of magnetic surfaces should be anti-symmetric from one side to the other of the resonant surface where the island is located [7], for this reason we expect to find the fluctuation phase jump right at the position of the dark surface.

In Figure 5 the location of phase jump detected by the algorithm is shown as a function of time, and a contour plot of magnetic q profile has been over laid for reference. The q profile displayed is inferred from the EFIT equilibrium code reconstruction constrained by Motional Stark Effect (MSE), polarimetry, and pressure profiles data. ECE radii are also calculated using the reconstructed equilibrium magnetic field. In the plot the main $n = 1$ NTM localized in both the high field side at 2.7m and the low field side at 3.4m is visible. The uncertainty on mode position is about 0.031m, that is the average distance between the two neighbouring channels that enclose the phase jump. This localization is not in perfect agreement with reconstructed q profile, that does not show any $q = 2$ surface at that time, but on the other hand this surface has to be present in the plasma since the related resonant mode is present.A secondary track is also present at the LFS and partially at the HFS, this track is localized between the reconstructed $q = 2.5$ and $q = 3$ surfaces, a similar experimental behaviour is reported in [10].

An m number analysis from magnetic coils at different poloidal angles was performed during the transition time interval between $n = 3$ mode to $n = 1$, the result is shown in Figure 6. Considering these measurements it is important to bear in mind that this kind of calculation has always been difficult in JET, due to poloidal asymmetry in the coils position, and it systematically overestimates the m number, compared to other m deduction methods.

The calculated m for the $n = 3$ NTM is around 9, and the best fitted m for the $n = 1$ NTM is around the value of 2.5, after a short phase of $m = 3$, while both the modes are present. This result, taken within the uncertainties described above, can give some hints about the physics we are observing. In fact the m analysis for the $n = 1$ NTM gives a mode which is neither a pure $m = 2$ nor a pure $m = 3$ harmonic, but could be a superposition of both the two harmonics, and in the following section we will give other arguments for this statement.

To understand the meaning of the more external track around 3.6m, let's call it second track from now on, a very important piece of information comes from the profile of plasma toroidal rotation frequency. In fact the magnetic frequency of a NTM in the first approximation depends on plasma rotation frequency at the resonant surface, and the resulting expression for mode frequency is $\omega = n\omega_{\phi}(R_{res}) + m\omega_{\theta}(R_{res})$. A more detailed approach is used in [11].

The picture could be then completed using the information contained in Figure 7, in which the temporal evolution of toroidal rotation radial profile, measured with Charge Exchange Spectroscopy (CXS), is shown. The first part of the heating phase exhibits a monotonic rotation profile from the plasma edge to the core. At 5.55s the doubling of n=3 NTM amplitude is followed by a modification of the rotational shear, with the creation of a low shear region between 3.4m and 3.6m in major

radius. The rotation flattening in this zone, which therefore appears to be linked to the n = 3 NTM, has the effect of modifying the rotation profile to the boundary conditions that favour further MHD onset. In the third part of the heating phase, from 6.6s on, the discharge is seriously affected by the onset of the large 2/1 NTM, with a significant drop in confinement. A larger effect on toroidal rotation is observed as well, in fact a zone with zero or even weak negative rotational shear is created, with an off axis rotation minimum around 3.36 meters, in agreement with the position of the main track of the 2/1 NTM. The difference between black line and red line is very close to uncertainty of the measurement (~5%), so, even if the relative behaviour of different radial measurements is clear, further investigations to confirm the actual magnitude of negative rotational shear are needed.

3.2 N = 2 NTMS

In this section the $n = 2$ mode will be considered, which is typically weaker than the $n = 1$ mode but occurs more frequently. As an example, we present the analysis of Pulse No: 76893 which is characterized by a 1.3MA plasma current, a 1.7T toroidal field, $\beta_n = 3$, and an hybrid scenario with a high triangularity configuration and an external input power of approximately 12MW of neutral beam, the input power and b_n traces are shown in Figure 8 upper and mid plot.

This scenario has a flat q profile in the plasma core, with a minimum value of q around 1, for this reason it is prone to q = 1 fishbone and sawtooth activity, and it is frequently affected by 3/2 and 4/3 NTMs as well. While fishbones are not dangerous for plasma global confinement, NTMs can indeed spoil plasma performances, as shown in Figure 8, where the increase in n = 2 signal amplitude at 6.2s (lower plot) is coincident with a large decrease in b_n (mid plot), despite the input power is raised (upper plot).

From the magnetic spectrogram in Figure 9 q = 1 activity is present at 13-14 kHz from 4.4s on, but it is not recognized by the tracking algorithm as a continuous mode, and it is then discarded (only the first longer sawteeth periods are kept). The frequency of this activity is suddenly reduced to 7-8 kHz after the onset of a $n = 2$ NTM at 6.2s, which lasts till the end of the heating phase.

The mode radial localization can be seen in Figure 10, in which two main tracks can be seen around 2.5m and 3.45m, in good agreement with the position of q = 1.5 surface within the error bars of the ECE channels position. Another $n = 2$ track in the LFS can be seen in this case as well, around 3.7m, and it appears from the beginning of the n = 2 NTM life. The $n = 1$ quasi-continuous activity can be localized as well at 2.8m and 3.25m, but only in the first part, when no NTMs were present. On the other hand during the NTM phase some sporadic n = 2 points are detected at the same position of previous q=1 activity, this could be due to the coupling of q = 1 activity with the $n = 2$ NTM (the latter has exactly twice the frequency of the former) observed in the spectrogram.

For this pulse the rotation profile behaviour has been studied as well, and again a clear correlation between $n = 2$ mode onset and a sudden decrease of toroidal rotation frequency is observed, this can be seen in Figure 11, where the rotation frequency evolution in function of time is shown for four different CXS channels. But the action of the mode on the rotation is more complicated than an

overall damping of the whole profile, in fact again a localized damping at 3.37m is experienced (red line in Figure 11), which creates again a non monotonic rotation profile.

In this case the distance of the local minimum of rotation from the mode position is about 10cm, and the distance from reconstructed q = 1.5 surface is about 15cm.

4. DISCUSSION

The experimental observations of the second external phase jump in the low field side, which were possible thanks to the newly implemented coherence tool, require a physical explanation which has to be compatible with the plasma rotation behaviour as well. In this section some possible explanations will be proposed, and their consistency with ECE radial profile and toroidal rotation data will be verified.

Once checked for a high coherence level in correspondence to the secondary jump, one of the possible explanations is a one to one correspondence between coherence phase p jumps and magnetic islands, in other words, this statement would imply the presence of a secondary magnetic islands chain in the plasma. This idea is sensible, since the presence of the main $m = 2$ island field resonant on q = 2 surface produces an $m = 2+1$ resonant sideband field that might cause forced magnetic reconnection in the q = 3 resonant surface. Accordingly to [11] this could happen only if the difference in toroidal rotation frequency between the two surfaces is small enough, and the secondary island should be born phase locked to the main one, in other words it should have zero toroidal rotation in the frame of the moving main mode.

On the other hand the double island structure gives rise to a slightly complicated picture, and it is certainly worth looking for the existence of a simpler idea that could satisfy the experimental observation as well. Let's then consider a double mode structure, similar to the one considered so far, but with the only difference that the $m = 2+1$ sideband has a simple kink structure without any magnetic island. It would be interesting to check if such a mode structure, simpler than the double island one, is still able to reproduce a coherence phase as the one which is observed experimentally in the data previously shown.

To make this test we artificially built an ECE fluctuation signal with the desired radial profile, and we used it as an input of the analysis coherence algorithm, to check if the output was similar to the real measured phase profile. In this process we could take large advantage from the fact that ECE radiometer line of sight is slightly off-axis, in fact this means that the poloidal angle θ is also varying along the line of sight, and then the phase profile changes along the major radius with a dependence of the form $m\theta(r)$, with r the radial coordinate along the ECE line of sight. Then knowing $\theta(r)$ from the previously used magnetic equilibrium reconstruction, and given the slope of the measured phase profile, we can extract information about the m number of the modes.

The ECE profiles used as first guess to reproduce the measured phase were the sum of two different profiles, the main one which had an oscillation profile of the form:

$$A_1(R)e^{-\varphi_1(R)}$$

with $A_1(R) = A_1\left(e^{\frac{(R-c_{11})^2}{2\cdot w_1^2}} + e^{\frac{(R-c_{12})^2}{2\cdot w_1^2}} \right)$ and $\varphi_1(R) = \varphi_1 + m_1\vartheta(R) + J_1(R)$

Where the poloidal angle q has a radial dependence $\theta(R) = \tan^{-1}\left(\frac{R-X_0}{Z_0}\right)$, R is the radial coordinate along the line of sight, X_0 is the radial position of the central axis and Z_0 is the vertical distance from ECE line of sight to plasma central plane.

The modelled amplitude profile has a double Gaussian shape, initially centred on the two radial points in which the LOS crosses the q = 2 surface (c_{11} and c_{12}) , and with a width w_1. (Figure 12, upper plot). This double Gaussian shape was chosen to give a good support to very localized modes, as NTMs can sometimes be, keeping still the possibility to fit well a rather broad profile.

The phase profile is composed instead by an initial phase value φ_1, plus a phase variation related to the radial variation of the poloidal angle and to the mode *m* number m_1= 2. Then, since it is expected the mode having tearing characteristic, a phase jump term J_1 was added which simulates the tearing behaviour, i.e. adds a p jump in the positions c_{11} and c_{12} where the main mode is localized.

For the secondary mode more than one shape for phase profiles has been tested, both with tearing behaviour or with kink behaviour, and amplitude profiles similar to the main mode ones, but centred at different radii and with different *m* number values. We show now the equations for a non tearing secondary component:

$$A_1(R)e^{-\varphi_1(R)}$$

with $A_2(R) = A_2\left(e^{\frac{(R-c_{21})^2}{2\cdot w_1}} + e^{\frac{(R-c_{22})^2}{2\cdot w_1}} \right)$ and $\varphi_2(R) = \varphi_2 + m_2\vartheta(R) + J_1(R)$

To determine the best value of the initial parameters for the reconstructed profile, a non linear least χ^2 multi-parameter fit has been used on the experimental phase profiles, using coherence amplitude profile as weighting factors.

As it can be noticed in Figure 13, the experimental phase profile can be well reproduced also with the *m* = 2 tearing plus *m* = 3 kink configuration, given a particular relation between the initial phases of the two different modes, and given a zone outside the main resonant component in which the fluctuation amplitude of the sideband is considerably larger than the amplitude of the main mode.

The best fitted values for the fitting parameters are:

A_1 (a.u.)	A_2(a.u.)	j_1(rad)	j_2(rad)	c_{11} (m)	c_{12} (m)
8.299±0.368	3.850±0.171	−0.526±0.012	4.296±0.013	2.706±0.008	3.426±0.010
c_{21} (m)	**c_{22} (m)**	**w_1 (m)**	**w_2 (m)**	**m_1**	**m_2**
2.258±0.044	3.738±0.054	0.560±0.019	0.147±0.004	2.092±0.009	3.138±0.009

In this case the minimization has been performed only on the coherence phase radial profile, but the consistency of the process can be checked comparing the simulated fluctuation amplitude with the ECE fluctuation amplitude measured at mode's frequency (Figure 12, lower plot). The simulated overall amplitude is similar to the experimental one, although it exhibits larger peaks in correspondence to $m = 2$ mode resonant surface, but smaller average amplitude everywhere else. Anyway the fit can not return a quantitative value for mode amplitudes, since it is performed on coherence phase, which does not depend individually on the two amplitudes , but on the ratio of the two.

It is worth remarking that m_1 and m_2 are fitting parameters as well, but their final value is still near the initial one, even though they are not compatible with their nearest discrete value within the fit uncertainty.

A weakness of the model could be introduced by the choice of the shape of coherence amplitude, for example in Figure 12, upper plot, it is clear that the fitted amplitude profile for the $n = 3$ mode is very broad and spread in the whole plasma, and this is reflected also on the large error on c_{21} and c_{22} determination. An odd m eigenfunction should have zero amplitude in the center of the plasma, tough the fitted one is still large inside the plasma, this means that a more constrained function shape should be used in the fitting procedure. Perhaps a more meaningful function for mode structure might be deduced from the pressure fluctuation radial structure modelled in non linear magnetohydrodynamic calculations [12].

To check for the consistency of this method also a single m mode profile has been used as input function, with the impossibility to reproduce the experimental behaviour of the phase slope inside the main resonant surfaces, and also the second jump in the external zone.

A physical picture with two independent $m = 2$ modes was considered as well, and the result of the fit is shown in Figure 14. The quality of the fit is clearly worse than the previous one, in fact the model is unable to produce the right radial behaviour of the coherence phase even between the jumps. Furthermore the fitted m_2 value in this case is 2.567 ± 0.012, which is nearer to $m = 3$ value than $m = 2$ starting value.

A similar thing happens if we try to fit the experimental data modelling a double mode structure with $m = 2$ plus $m = 3$ modes, both with tearing characteristic. In Figure 15 the result of the fit is shown, the fit parameters converged towards a minimum point very close to the one obtained for the tearing-kink case, but the second outer jump due to the $m = 3$ tearing component (3.7m) is changing the total coherence phase in the outer part of the plasma, giving a worst overall result (note that radiation coming from R>3.8m is heavily affected by non-thermal effects, and consequently it is not reliable).

Each of the two hypothesis should be compatible with Rotation measurement results. The last would be well explained by the double island picture, in fact the generated multiple tearing structure should rotate at the same angular speed at different resonant radii, but being in clear conflict with the rotation shear induced in the plasma by external momentum injection, it could interact with the plasma itself via a torque, changing the rotation profile. The multiple tearing structure might act to

cancel out the differences in toroidal rotation between the islands, in this way the rotation frequency of the most internal mode can be lowered by the torque exerted by the external island, which can in turn be accelerated by the torque of the main one, to a level in which the total torque balance between magnetic torque exerted by the other island and kinetic torque due to natural plasma rotation will be zero.

This explanation foresees the action of a very localized braking mechanism as the one that is observed experimentally, since from the measurements the effect of the mode is to reduce the rotation frequency in the channel nearest to the mode radial position, while in the other regions of the profile rotation is less affected. The toroidal momentum input to the plasma remains unchanged with the appearance of the mode, though the zones in which the localized braking is active experience also the torque due to braking, the result of this mechanism might be a non monotonic rotation profile.

In the kink sideband picture drawing a clear link from mode behaviour to rotation data is less straightforward than in the double island picture. It is out of doubt that the mode has a clear impact on rotation, both in a localized and in a global way, tough the origin of the braking mechanism needs still to be understood, and the presence of an interaction between the mode and an external error field might be invoked.

In Figure 16 the q profile from the equilibrium reconstruction is shown, for Pulse No: 77590. The q profile is very broad and slightly reversed in the middle of the plasma, with a value of q_{min} slightly above 2, while it is increasing steeply going towards the edge. The fitted positions of the m = 2 ECE fluctuation maxima for the best fit case are over-plotted as dotted lines, while the positions of m = 3 maxima as dashed lines. It could be argued that m = 2 mode positions are not in perfect coincidence with the local minima in the q profile, and also that the positions of m = 3 mode in the low field side and high field side correspond to two different q values, but this is compatible with a systematic error in the total field determination, which affects ECE channel position at JET, and is now under investigation [8].

CONCLUSIONS

In this paper the presence of a multiple jump structure in ECE phase radial profiles has been documented in JET plasmas under different experimental conditions, and the consequences of this structure on plasma toroidal rotation has been analyzed.

Different hypothesis have been presented in order to explain the double phase jump experimental evidence, among these the most reliable is based on an $m = 2$ plus $m = 3$ structure. This hypothesis has been tested with an ad-hoc simple modelling of ECE fluctuation radial profile, which demonstrated a good agreement with experimental data.

It is worthwhile noting that both the two different m harmonics have been detected at the frequency of the mode, and for this reason could not be found previously with routine magnetic m analysis at JET. The insight on the radial mode structure given by the technique has indeed played a crucial role in the determination of the m mode structure as well.

The issue of the nature of the *m*=3 sideband is still open, in principle both a tearing structure and a kink structure could be adequate to describe the experimental evidence, even though the second one has proven to be much more effective in reproducing the experimental phase profile in a very good way. Being born at the same time of the main $m = 2$ component, and rotating at the same angular frequency, the $m = 3$ component appears to be an $m = +1$ toroidal sideband of the main NTM, which could not manage to cause forced reconnection at the $q = 3$ surface, since the $q = 2$ and $q = 3$ surfaces rotated toroidally at different frequencies.

A simple mechanism for the interaction of the mode itself with plasma rotation has been proposed as well, particularly for the double island case, which involves the torque that the two island exerts one on each other.

More investigations are needed to explain the rotation behaviour in the kink sideband case, but we think that a localized resonant damping can only partially reproduce the complex observed behaviour.

As future work a deeper study of modes radial structure impact on rotation should be performed, and in turn the effect of local reversal in the rotational shear on the discharge might be analyzed, to decouple the effects of heat transport across the magnetic island from rotation profile effects.

ACKNOWLEDGMENTS

This work, supported by the European Communities under the contract of Association between EURATOM and Consorzio RFX, EURATOM-ENEA Association, was carried out within the framework of the European Fusion Development Agreement. The views and opinions expressed herein do not necessarily reflect those of the European Commission.

REFERENCES

[1]. Chang Z *et al.,* 1995 *Physics Review Letters* **74** 4663

[2]. Buttery R.J, *et al.,* 2003*, Nuclear Fusion* **43** 69.

[3]. Challis C *et al.,* 2009, *36th EPS Conference on Plasma Physics, Sofia*, O5.057

[4]. Welch P, 1967, *IEEE transactions* **15**, issue 2 ,70-73

[5]. de la Luna E, *et al.,* 2004*, Review Scientific Instrum*ents **75**, 3832 1414

[6]. Cruz N, *et al.,* 2004, *Fusion Engineering and Design*, **71**, Issues 1-4, 167-173

[7]. Fitzpatrick R, 1993, *Nuclear Fusion* **33** 10

[8]. Buratti P, *et al.,* 2009, *36th EPS Conf. on Plasma Physics. Sofia,* P5.169

[9]. Mailloux J, *et al.,* 2009, *36th EPS Conference on Plasma Physics Sofia* P5.164

[10]. Buratti P, 2008, *35th EPS Conference on Plasma Physics Hersonissos,* ECA Vol.**32D**, P-1.069

[11]. Fitzpatrick R, 1995 *Physics of Plasmas* **2** 3

[12]. Maget P, *et al.,* "Modelling of (2,1) NTM threshold in JET Advanced Scenarios" submitted to *Nuclear Fusion*.

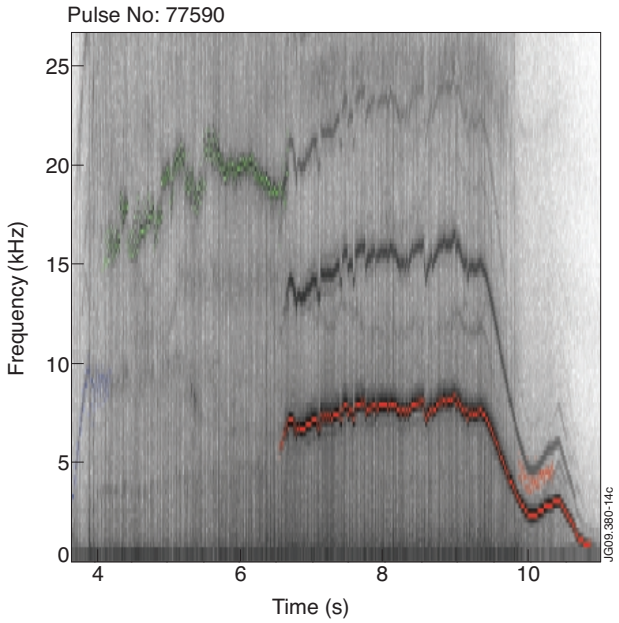

Figure 1: Spectrogram from a 1MHz bandwidth pick up coil for Pulse No: 77590. The different coloured tracks are the output of the mode tracking algorithm. Red tracks are linked to n = 1 activity, blue tracks to n = 2 activity and green tracks to n = 3 activity.

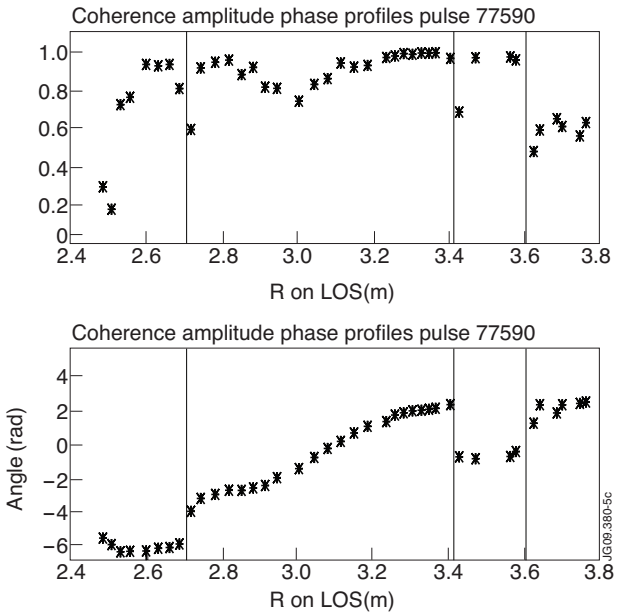

Figure 2: Coherence amplitude and phase radial profile n = 1. NTM in Pulse No: 77590 at t = 6.8s Dolid lines are positioned in the position of detected jump radii.

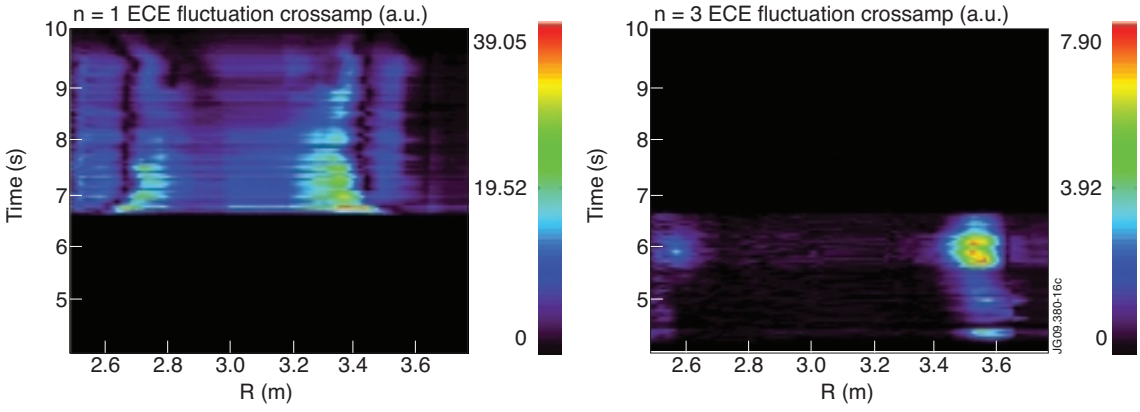

Figure 3: Contour plot of fluctuation cross-amplitude between magnetic a signal and all ECE channels, as a function of channel position and time at the frequency of the mode, for n = 1 and n = 3 modes respectively, for Pulse No: 77590.

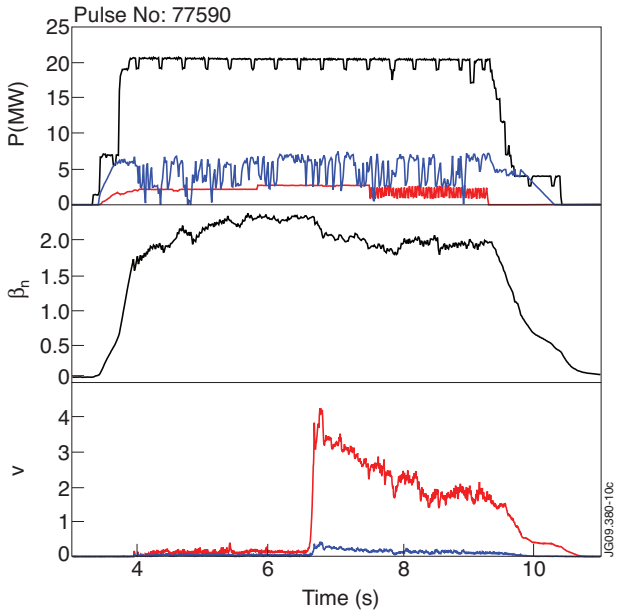

Figure 4: In the upper box the amount of NBI input power (black), ICRH (blue), LH (red) are shown for Pulse No: 77590. In the central box b_n evolution is shown and in the lower box the odd n (red) and even n (blue) integrated magnetic amplitudes are shown.

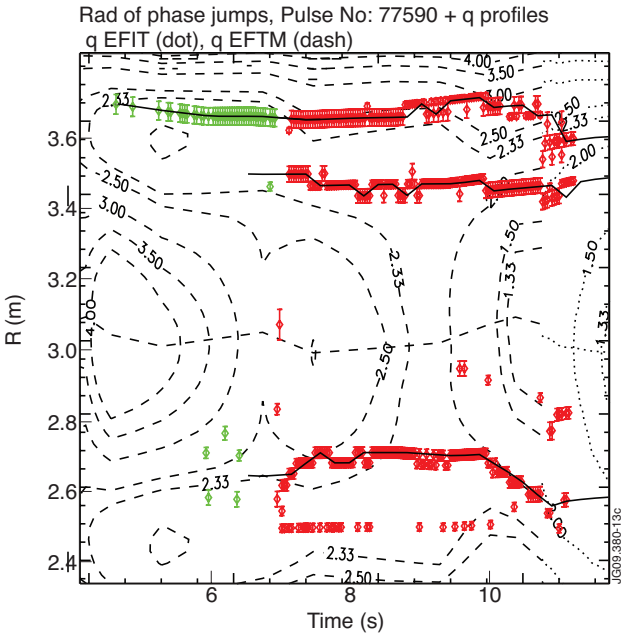

Figure 5: Mode position detected by ECE phase jumps, as a function of time and channels radii for discharge 77590. Red points are due to n=1 mode and green points to n=3 mode. The error bars are the distances between the two channels that enclose the phase jump. The contour plot of q-profile inferred from the EFIT reconstruction constrained by MSE, CXS and pressure data is plotted.

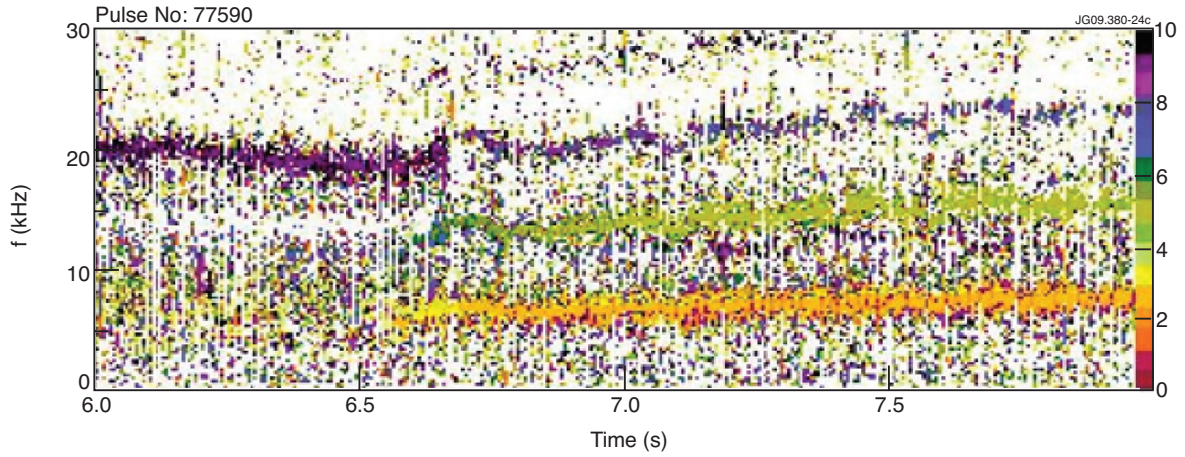

Figure 6: ***m number analysis from HFS 1 MHz bandwidth pick up coils for****Pulse No:* ***77590.***

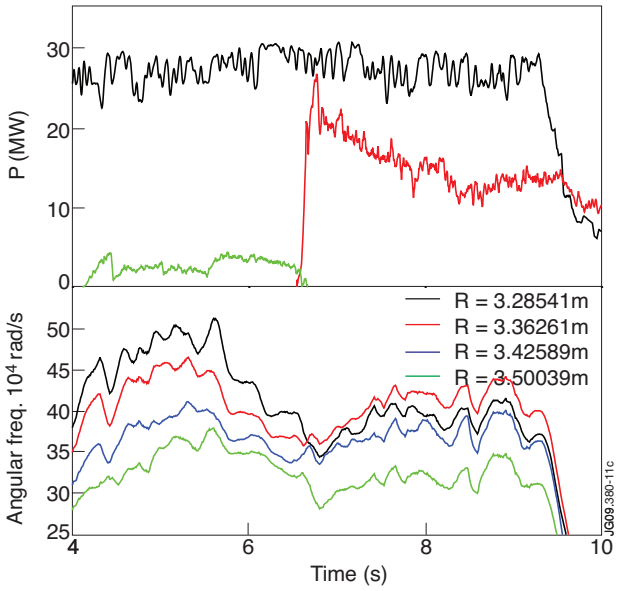

Figure 7: In the upper plot the total input power coupled to the plasma is plotted in black for Pulse No: 77590, n = 1 and n = 1 magnetic amplitudes are over plotted (a.u.). In the lower plot toroidal rotation evolution from Charge exchange spectroscopy is plotted for different radial positions in the plasma.

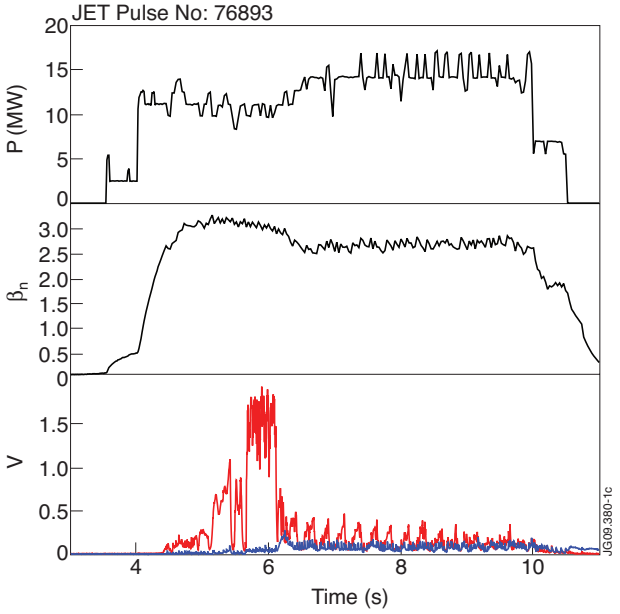

Figure 8: In the upper box the amount of NBI input power (black) is shown for Pulse No: 76893. In the central box β_n evolution is shown and in the third box the odd n (red) and even n (blue) integrated magnetic amplitudes are shown.

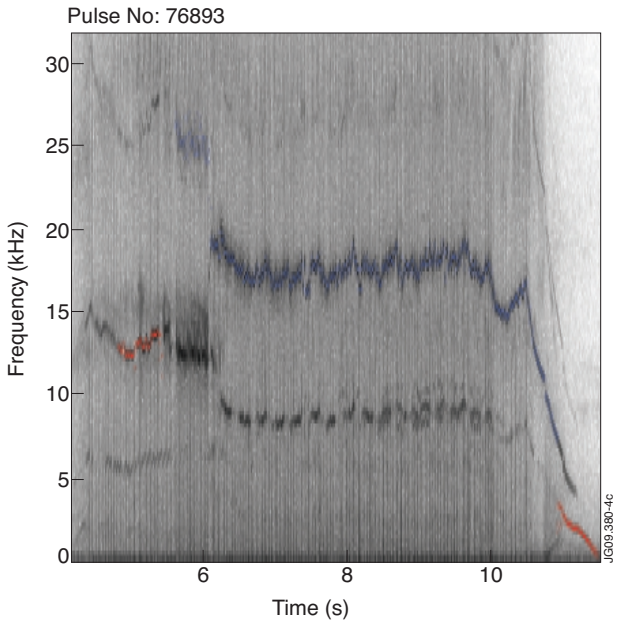

Figure 9: Magnetic spectrogram from a 1MHz bandwidth pick up coil for Pulse No: 76893. Red tracks are linked to n = 1 activity and blue tracks to n = 2 activity. The mode at 9kHz is not recognized as a continuous mode by the tracking algorithm, and then discarded

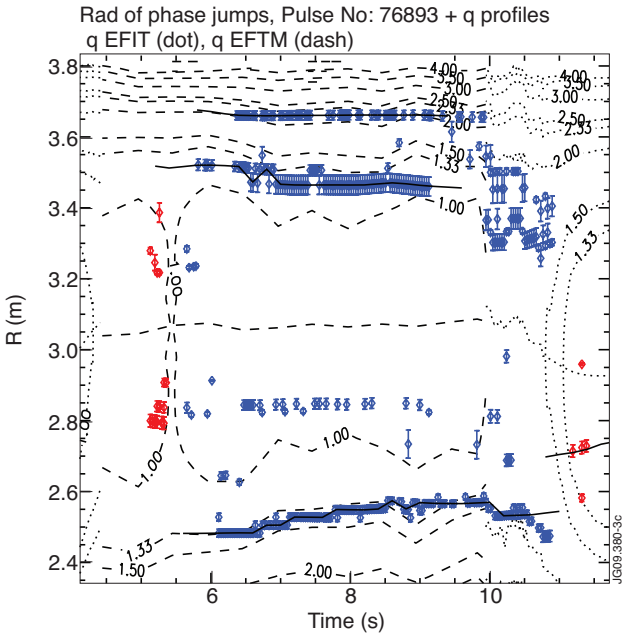

Figure 10: Mode position detected by ECE phase jumps, as a function of time and channels radii for Pulse No: 76893. Red points are due to n = 1 mode and blue points to n = 2 mode. The error bars are the distances between the two channels that enclose the phase jump. The contour plot of q-profile inferred from the EFIT reconstruction constrained by MSE, CXS and pressure data is plotted .

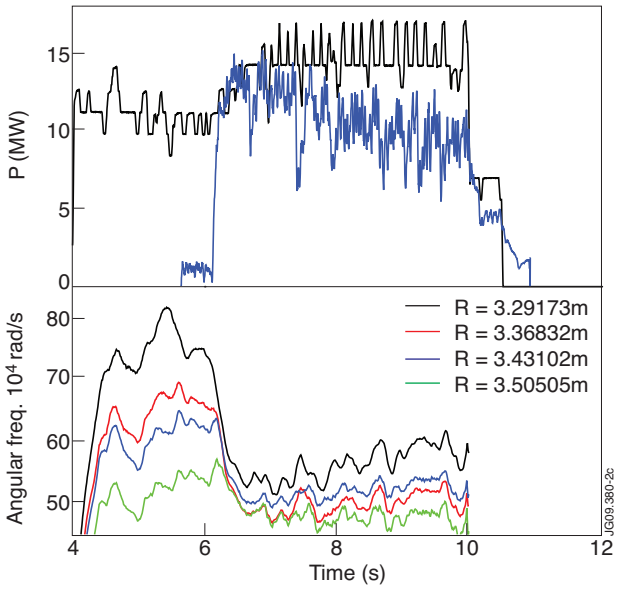

Figure 11: In the upper plot the total input power coupled to the plasma is plotted in black for Pulse No: 76893, and n = 2 magnetic amplitude is over plotted (a.u.). In the lower plot toroidal rotation evolution from Charge exchange spectroscopy is plotted for different radial positions in the plasma.

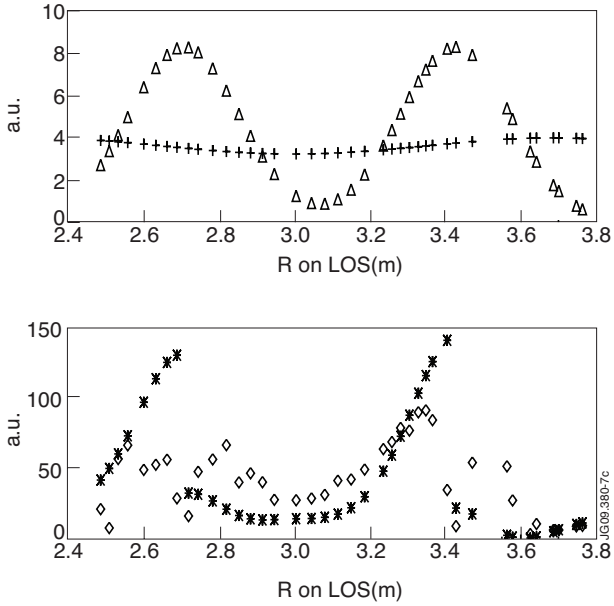

Figure 12: In the upper plot the radial oscillation amplitude profile is shown for Pulse No: 77590 at t = 8s, for the two different mode components reconstructed with fitted parameters. The amplitude profile for m = 2 component is shown as stars, while for the m = 3 component as crosses. In the bottom plot the total reconstructed amplitude (stars) is compared to the measured one (diamonds). The radii values are along ECE line of sight.

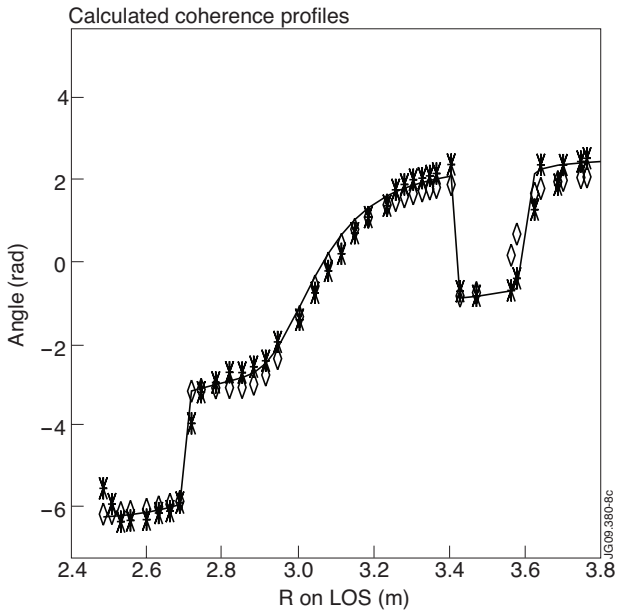

Figure 13: In this figure the phase profile built using initial guess values is shown (diamonds) for Pulse No: 77590 at t = 8s. Experimental points are shown as well (stars) and the fitted profile is over plotted as solid line. The radii values are along ECE line of sight.

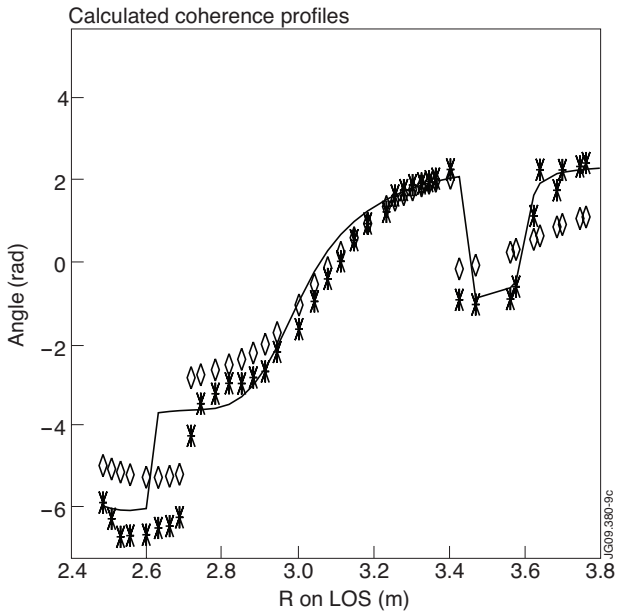

Figure 14: In this figure the phase profile built using initial guess values is shown (diamonds) for Pulse No: 77590 at t = 8s (two different m = 2 modes are supposed). Experimental points are shown as well (stars) and the fitted profile is over plotted as solid line. The radii values are along ECE line of sight.

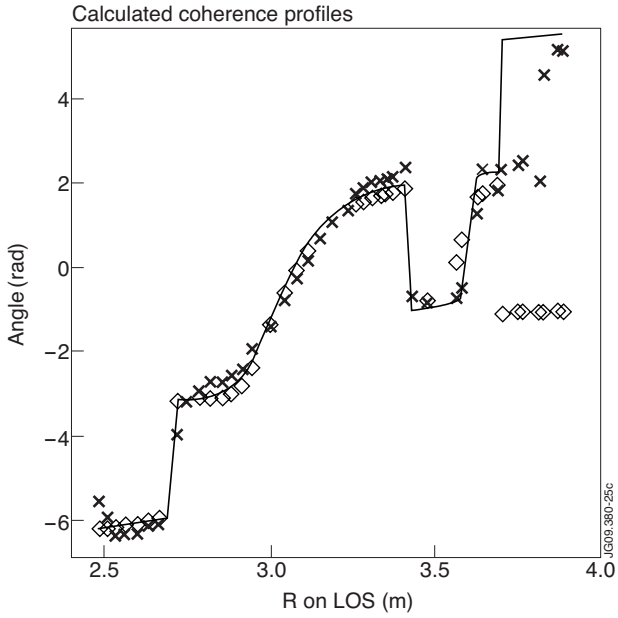

Figure 15: In this figure the phase profile built using initial guess values is shown (diamonds) for Pulse No: 77590 at t = 8s (for m = 2 and m = 3 both tearing). Experimental points are shown as well (stars) and the fitted profile is over plotted as solid line. The radii values are along ECE line of sight.

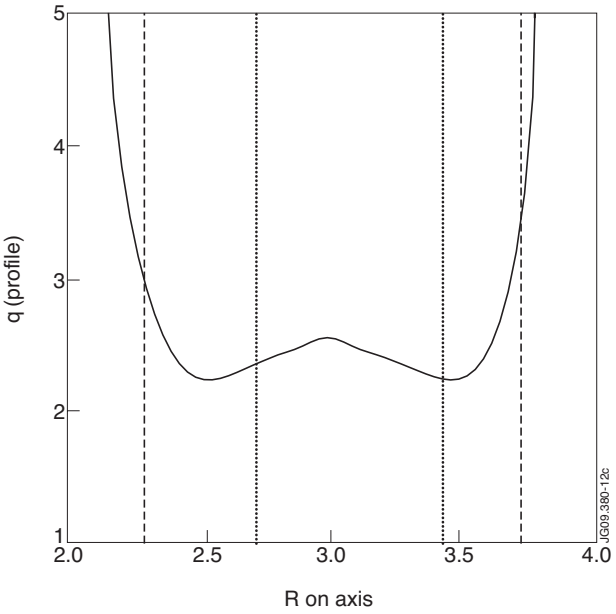

Figure 16: In the plot the magnetic q profile at t = 8s is shown for Pulse No: 77590. The dotted line is the position of the tops on the m = 2 double Gaussian, while the dashed line is the position of the m = 3 double Gaussian.